BJRS
BRAZILIAN JOURNAL OF RADIATION SCIENCES

doi.org/10.15392/2319-0612.2024.2760
2024, 12(4B) | 01-27 | e2760
Submitted: 2024-08-31
Accepted: 2024-11-15

Computational analysis of wax deposition in deep-water pipelines using nuclear techniques

Leite [a*], N. M.; Lira [a], C. A. B. O.; Rodriguez [b], A. G.

[a] Northeast Regional Nuclear Science Center, 50.740-540, Recife, Pernambuco, Brazil.
[b] Federal University of Pernambuco, 50.740-545, Recife, Pernambuco, Brazil.

*Correspondence: nalber2009@gmail.com

Abstract: Wax deposition in oil pipelines is a problem that affects flow assurance because it restricts production and, in more extreme cases, causes pipeline blockages. This problem occurs more frequently in offshore environments, where most of Brazil's reservoirs are located and where the ocean temperature at great depths is around 5°C. Detecting the wax layer on the inside walls of pipelines at an early stage avoids unscheduled stoppages and major economic losses. Among the various methods and techniques found in the literature for monitoring wax deposition, nuclear techniques are distinguished by the fact that their use does not interfere with the physical integrity of the pipeline, by the non-intrusive and indirect (non-contact) mode of operation and, therefore, does not affect the oil transportation process. This paper presents a computational model using the Monte Carlo N-Particle 6 (MCNP6) code and the gamma radiation transmission profiling technique to detect the presence of wax on the inner walls of pipelines used for deepwater oil transportation. The results of this study show that the model can detect the presence of up to 5% wax (in relation to the internal radius of the pipeline) with an accuracy of 7.4% in pipelines used in deep waters.

Keywords: wax deposition, nuclear technique, gamma radiation, Monte Carlo method.

SBPR

BJRS
BRAZILIAN JOURNAL OF RADIATION SCIENCES

doi.org/10.15392/2319-0612.2024.2760
2024, 12(4B) | 01-27 | e2760
Submitted: 2024-08-31
Accepted: 2024-11-15

Análise computacional da deposição de parafina em oleodutos de águas profundas utilizando técnicas nucleares

Resumo: A deposição de parafina em dutos de petróleo é um problema que afeta a garantia de escoamento porque restringe a produção e em caso mais extremos, causa obstrução dos oleodutos. Esse problema ocorre com maior frequência em ambientes offshore, onde se encontram a maior parte dos reservatórios brasileiros em que a temperatura do oceano, em elevadas profundidades, é cerca de 5°C. Detectar a camada de parafina nas paredes internas dos oleodutos em seu estágio inicial evita paradas não programadas e grandes perdas econômicas. Dentre os vários métodos e técnicas encontrados na literatura para o monitoramento da deposição de parafina, as técnicas nucleares se diferenciam pelo fato de seu uso não interferir na integridade física do duto, pelo modo de operação não intrusivo e indireto (sem contato) e, portanto, não afeta o processo de transporte do petróleo. Este trabalho apresenta um modelo computacional utilizando o código Monte Carlo N-Particle 6 (MCNP6) e a técnica da perfilagem por transmissão da radiação gama para detectar a presença de parafina nas paredes internas de oleodutos utilizados no transporte de petróleo em águas profundas. Os resultados deste estudo mostram que o modelo é capaz de detectar a presença de até 5% de parafina (em relação ao raio interno do oleoduto) com uma exatidão de 7,4% em oleodutos utilizados em águas profundas.

Palavras-chave: deposição de parafina, técnica nuclear, radiação gama, método de Monte Carlo.

SBPR

1. INTRODUCTION

Flow assurance refers to the economic and safe transmission of hydrocarbon fluids during oil and gas production. Production in offshore fields, especially in the deep and ultra-deep waters of pre-salt fields, poses distinctive challenges for flow assurance. These include the deposition of wax (C_nH_{2n+2}) along the extensive production pipelines, due to the deep-water depths and the consequent temperature profile along the flow[1].

In oil reservoirs, waxes are typically initially solubilized in the liquid phase of the oil in an equilibrium state. This is because oil temperatures in reservoirs are in the range of 70 to 150°C. This condition changes when the oil is extracted from the reservoir[1]. When it enters the production line, at a temperature of approximately 70°C, the oil begins to cool along the pipeline due to the difference in temperature in relation to the external environment. This problem occurs more frequently in offshore environments, where the ocean temperature at great depths is around 5°C. As the oil cools and reaches the Wax Appearance Temperature (WAT), the process of wax precipitation and subsequent deposition begins (Figure 1)[2].

Figura 1: Melting point of wax depending on the number of carbons

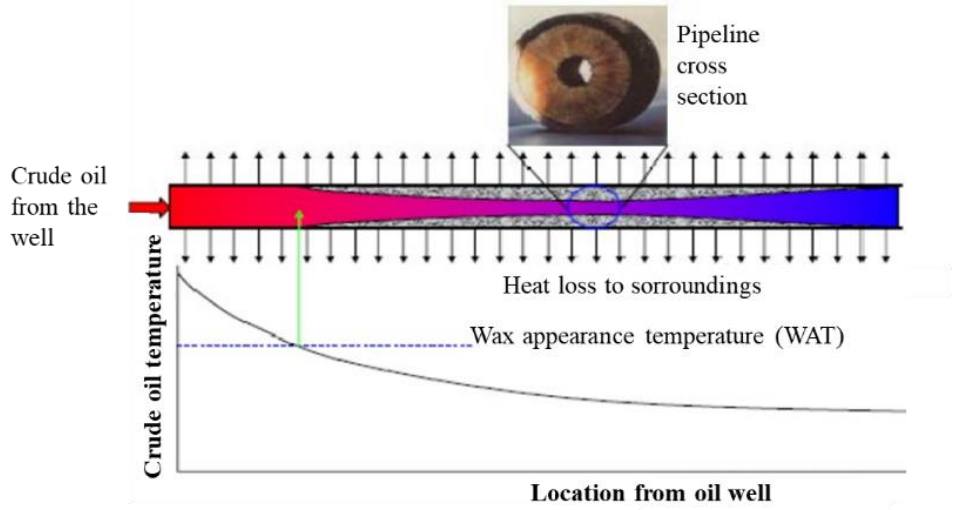

Source: Adapted from [3].

Initially, the deposition rate is high but decreases as more wax is deposited on the surface of the pipeline. This is because the thickness of the wax layer acts as a thermal insulator, reducing the effective temperature differential[4].

There are several wax deposition mechanisms where, even amid contradictions regarding the relevance of each mechanism, there is unanimity in considering molecular diffusion as the dominant mechanism in the deposition process[2].

Wax deposition occurs according to the type of flow pattern and depends on the flow velocities of the two-phase fluids (crude oil and natural gas). In addition, deposition occurs only along the pipeline wall in contact with a waxy crude oil and an increase in the fluid mixing velocity results in harder deposits, but with a smaller deposit thickness[5].

The problem of wax deposition occurs in the various stages of oil handling, during production, transportation and refining. Petrobras, which is internationally recognized as having the technology to explore and produce in deep and ultra-deep waters, frequently encounters problems related to the formation and deposition of wax in its subsea lines[6]. The problem can cause a loss of millions of dollars a year worldwide through the enormous cost of prevention and remediation, reduced or postponed production, shut-in of wells, replacement and/or abandonment of pipelines, equipment failures, extra power requirements and increased labor needs[7].

The use of pigging is one way in which wax removal is commonly carried out in oil fields. This equipment is introduced into the pipes and displaced by the flowing fluid itself or by another fluid injected for this purpose, with the aim of removing the wax deposits[8]. In addition to the use of pigging, other measures adopted by Petrobras consist of the use of a Nitrogen Generating System (SGN), which generates an exothermic chemical reaction based on nitrogen and the use of chemical additive injections to dissolve or inhibit the formation of deposits[9].

Earlier identification of wax deposits will reduce the cost of maintenance, minimizing both unnecessary pipe replacements and plant shutdowns for inspection[10]. As oil and gas production moves into deeper and colder waters, it becomes increasingly imperative to properly identify wax precipitation conditions and predict wax deposition rates to optimize the design and operation of multiphase subsea production systems[7].

The literature presents various wax monitoring techniques, such as: heat pulse monitoring[11]; high-pressure ultrasonic detection[12]; electrical capacitance tomography[13]; a multi-point sensor based on a resistive temperature detector[14] and a Data Acquisition Module for pigging (MAD-pig)[15].

Nuclear techniques are distinguished by the fact that their use does not interfere with the physical integrity of the pipeline, i.e. they operate in a non-intrusive and indirect way (without contact) and therefore do not affect the oil transportation process. According to the existing state of the art, among all the non-contact control methods, only the radioisotope method has shown efficiency when used with heterogeneous currents, which include oil flows, being the method capable of detecting the formation of the wax layer in the early stages and creating automated systems to control the formation of wax deposits[16].

The following nuclear techniques for monitoring wax deposition stand out: gamma radiation Compton scattering technique[17]; gamma radiation transmission technique[18]; neutron backscatter technique[19] and the neutron capture gamma ray technique[19].

In view of the above, the aim of this paper is to develop a computer model based on the gamma radiation transmission profiling technique to identify the presence of wax in deepwater oil pipelines.

2. MATERIALS AND METHODS

2.1. Transmission of gamma radiation

Gamma radiation is electromagnetic in nature and due to its wave-like nature, lack of charge and rest mass, it can penetrate a material, traveling through great thicknesses before undergoing the first interaction. This penetrating power depends on the probability of interaction for each type of event, which can absorb or scatter the incident radiation[20].

The attenuation of a narrow, parallel beam of monoenergetic photons penetrating a thin slab of homogeneous material follows the Lambert-Beer exponential decay law[21] according to Equation 1.

$$I = I_0 e^{-\mu\lambda} \tag{1}$$

Where I is the intensity of the transmitted beam, I_0 is the intensity of the initial or incident beam, λ is the thickness of the absorber and μ is the linear attenuation coefficient, which expresses the probability of photon interaction per unit path length in the absorber. The linear attenuation coefficient is strongly dependent on the radiation energy, density and atomic number of the absorber. It is the sum of the contributions of several independent interaction mechanisms: photoelectric absorption, Compton scattering, pair production and Rayleigh scattering[21].

In the case of a material composed of n layers of different elements and thicknesses, the intensity I of the transmitted beam is given by Equation 2[20].

$$I = I_0 e^{-\sum_{i=1}^{n} \mu_i \lambda_i} \tag{2}$$

From the Lambert-Beer Law (Equation 1) and according to Knoll[22], the relative intensity is the ratio between the number of transmitted photons I and the number of incident photons I_0 according to Equation 3

$$\frac{I}{I_0} = e^{-\mu\lambda} \tag{3}$$

Figure 2 shows a narrow beam of monoenergetic photons from a collimated gamma radiation source reaching a detector after passing through an absorber material of varying thickness

Figure 2 : Representation of the exponential transmission curve of gamma radiation for a monoenergetic beam

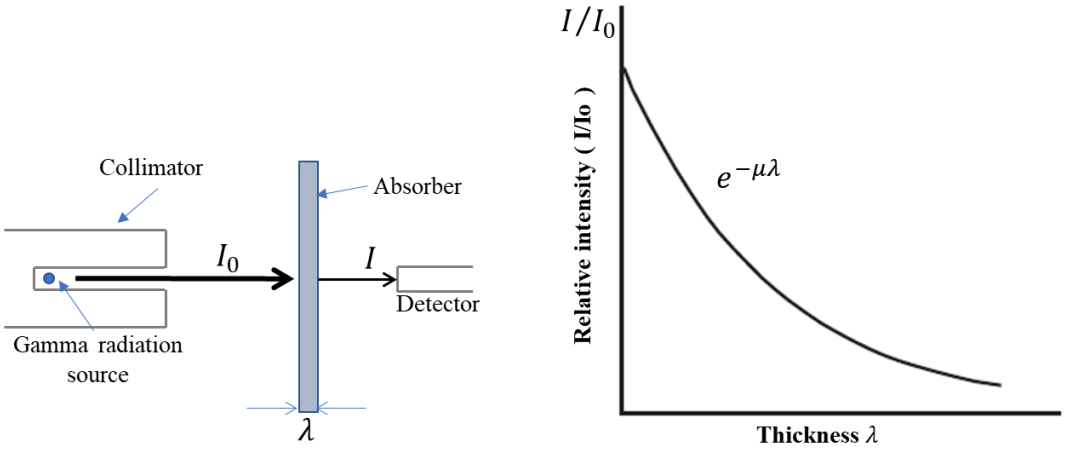

Source: Adapted from [22].

As shown in Figure 2, the result of Equation 3 is an exponential curve of the thickness λ versus the relative intensity $\frac{I}{I_0}$. However, the narrow beam configuration of monoenergetic photons or "good geometry" is rarely achieved in a realistic measurement system, because a portion of the photons that interact outside the beam defined by the source/detector geometry is scattered towards the detector aperture and contributes to the measured intensity. As the detector can respond to gamma rays directly from the source to gamma rays arriving at it after scattering at the absorber or to other types of secondary photon radiation, the conditions leading to simple exponential attenuation (Figure 2) are therefore violated in wide beam or "poor geometry" measurements because of the additional contribution from

secondary gamma rays[22]. To resolve this, the factor $B(\lambda, E_\gamma)$, called buildup, is introduced[22]. Equation 3 becomes:

$$\frac{I}{I_0} = B(\lambda, E_\gamma)e^{-\mu\lambda} \quad (4)$$

Where λ is the thickness of the absorbing material and E_γ is the energy of the gamma radiation photon.

2.2. Gamma radiation transmission profiling technique

It consists of moving a source-detector assembly so that the gamma radiation beam scans the section of the duct by means of a pre-established step (Figure 3a)[23].

Figure 3 : Gamma radiation transmission profiling technique

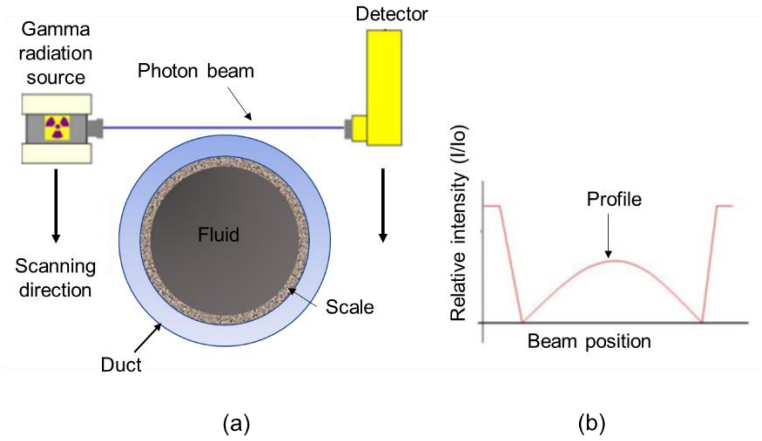

Source: Adapted from[24]

The relative intensity $\frac{I}{I_0}$ count is recorded at each beam position, as shown in Figure 3b. The beam is attenuated according to the Lambert-Beer Law - since different types of absorbers are involved, Equation 2 applies - at each position along the pipeline cross-section. The most used radioisotope sources are ^{241}Am, ^{133}Ba, ^{137}Cs, ^{60}Co and ^{192}Ir[21].

Advantages of this technique:

- It operates in non-intrusive mode and without contact with the pipeline structure.

- Its application does not interrupt oil transportation.
- It uses a radioisotope that intrinsically has a long duration (longer half-life), which makes its operation more reliable than other techniques whose operation depends on other energy sources.
- It uses a lower energy radioisotope source when compared to neutron backscatter and neutron capture gamma ray techniques[21].

Its limitation, however, concerns the conditions of the oil during profiling as it is a heterogeneous and time-varying mixture[25]. However, it can operate in conjunction with a device capable of continuously monitoring oil products, including density and flow velocity measurements[18].

2.3. Monte Carlo method

The Monte Carlo method is a mathematical tool commonly used in various areas of science and engineering to simulate problems that can be represented by stochastic processes. Due to its random nature, the transport of radiation through materials is a complex process that is often impossible to solve analytically. Monte Carlo methods simulate the random trajectories of individual particles (e.g. photons) using computer-generated pseudo-random numbers[26].

By simulating a large number of trajectories, information can be obtained about average values of macroscopic quantities, such as energy deposition in predefined volumes, for example in a radiation detector[21]. Any Monte Carlo calculation begins by creating a model that represents the real system of interest. The interactions between the radiation and this model are then simulated by randomly sampling the Probability Density Functions (PDF) that characterize this physical process. As the number of simulated particle histories increases, the quality of the system's average behavior improves, characterized by a reduction in the statistical uncertainties of the quantities of interest[26].

There are a variety of Monte Carlo simulation codes available, but they all have four main components in common: The geometry definition interface, the cross-section data (or shock section) for all the processes considered in the simulation, the algorithms used for radiation transport and, finally, the interface for analyzing the information obtained during the simulation[21].

2.3.1. Code MCNP6

One of the Monte Carlo codes is Monte Carlo N-Particle (MCNP), described as a general-purpose three-dimensional simulation tool that carries 37 different types of particles for criticality, shielding, dosimetry, detector response and many other applications[27]. In this work, the MCNP6 code version 1.0 will be used.

To carry out a simulation in the MCNP6 code, an input file must be prepared according to the code model, containing all the information needed to describe the problem[28]:

- Cell card, where the geometry of the problem is described, using combinations of predefined geometric shapes, such as planes, spheres, cylinders, etc. This card should also contain materials whose compositions are on the data cards and their respective densities. Another piece of information that can and should be included with the data cards is the importance of each cell defined on the importance card.
- Surface card: where the geometric shapes to be used in the problem geometry are selected. For this, mnemonic characters are used indicating the type of surface and then the coefficients of the equation of the selected surface.
- Data card: where the physical data of the problem is described. It is made up of the following cards: Mode card, which defines the type of radiation used in the problem, using the letters P (Photons), E (Electrons) and N (Neutrons); Material card, which defines the types of materials and their respective atomic weight fractions, as well as the cross-section library of the elements; Source card, which

defines the type, energy, position, direction and particle of the radiation source; Tally card, which defines the type of count, i.e. what you want to write in the output data at the end of a run.

- Cutoffs, where the limits imposed by the user for completing the execution of the problem are presented, such as number of stories or Number of Particles Started (NPS), time, energy, etc.

2.3.2. Error estimation

The result of the chosen tally is printed in the output file accompanied by the relative error R defined according to Equation 5[28].

$$R = \frac{S_{\bar{x}}}{\bar{x}} \tag{5}$$

Where $S_{\bar{x}}$ is the estimated standard deviation of the mean $\bar{x}$. R is a convenient number because it represents statistical precision as a fractional result in relation to the estimated mean. For a well-behaved tally, R will be proportional to $\frac{1}{\sqrt{\mathrm{N}}}$, where N is the number of stories or NPS[28].

Guidelines for interpreting the quality of the confidence interval for various values of R are listed in Table 1.

Table 1: Guidelines for interpreting the relative error R

Range of R	Quality of the Tally
0.5 to 1.0	Garbage
0.2 to 0.5	Factor of a few
0.1 to 0.2	Questionable
0.05 to 0.1	Generally reliable except for point detector
<0.05	Generally reliable for point detector

Source: [28]

In this study, R<0.01 was considered so that wax detection was within a confidence interval equal to or greater than one standard deviation.

2.4. Computational model of a deep-water subsea pipeline

To achieve the objective of this work, a computational model was developed that represents a small section of a submarine oil pipeline located in deep waters. This model was implemented in the MCNP6 code version 1.0. This code also implemented the gamma radiation transmission profiling technique. Figure 4 shows the model schematic.

Figure 4 : Geometry of deepwater subsea pipeline model

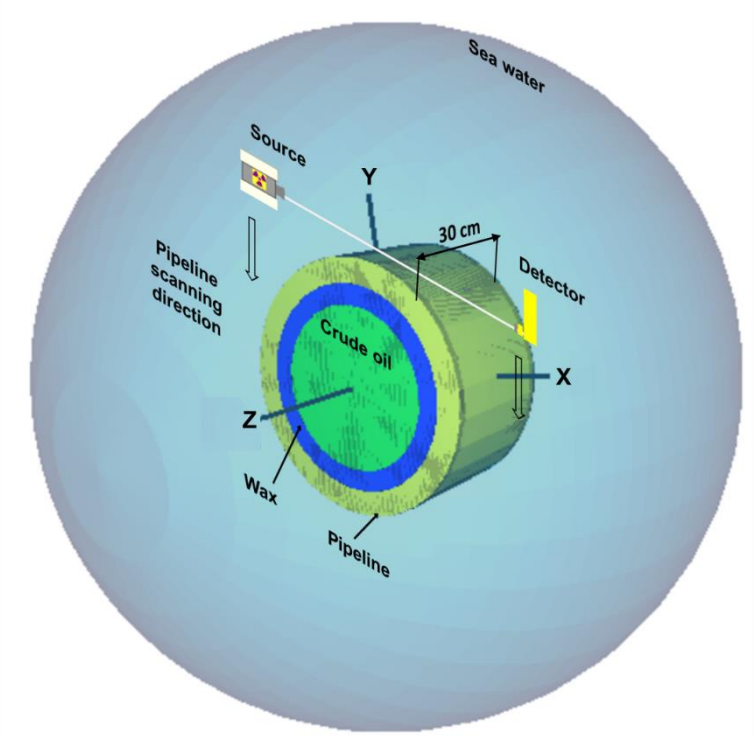

The characteristics of the materials to justify their chemical composition and density that will be used in the input files are as follows:

Seawater: Salinity of 4% of mass fraction of sodium chloride (NaCl)[29]. Its density is 1.047 g/cm^3[30].

Pipeline: Deep-water oil pipelines must be designed to withstand higher pressure applied by the external environment, implying the use of pipelines with a smaller diameter/thickness ratio and higher-strength materials[31]. In general, API X-60 or X-65 grade steels are adopted for projects of rigid pipelines, installed at depths above 1000 m[32]. This study will consider the oil pipelines described in Table 2, where the greatest wall thickness was considered.

Table 2 : Pipelines considered for deepwater use

Outer diameter [in]	Outer radius [cm]	Wall thickness [cm]
8	10.95	2.30
12	16.19	3.33
16	20.32	4.05
20	25.40	5.00
24	30.48	5.95

Source :[33]

Due to the high percentage of iron in steel compared to other elements[34], for simulation purposes in MCNP6 it was feasible to adopt only iron as the composition of steel[24]. The density of this element is 7.874 g/cm^3[35].

Crude oil: In Brazil, the National Agency of Petroleum, Natural Gas and Biofuels (ANP) shows that oil classified as medium represents the highest percentage, around 90%[36]. The increase in the API grade from 24.5º in 2010 to 28º in 2020 shows that the quality of crude oil produced in Brazil is close to the light oil classification range[37]. Since the chemical composition of oil classified as medium was not found in this research, light oil will be used, whose chemical composition and density (0.875 g/cm^3) will be used[35].

Wax: For the wax that adheres to the internal walls of the pipeline to be detected by gamma radiation, its density must be above that of crude oil[38]. Waxesns that fit this condition are those that have 25 to 50 or more carbons in their molecular structure in their chain[39]. Therefore, for this study, wax $C_{25}H_{52}$ will be used. Its density is 0.93 g/cm^3[35].

Detector: In this study, the Sodium Iodide scintillation detector doped with Thallium (NaI(Tl)) was used. For its use in deep waters, it must be placed in an airtight container, because it is hygroscopic[22]. This device has been used in aquatic environments[40]. Its density is 3.67 g/cm^3[41].

The cross sections of the chemical elements were selected from the MCPLIB04 photoatomic data library, which is a library based on ENDF/B-VI data[28].

2.4.1. Source Specification

Most experiments with the gamma radiation transmission profiling technique used the radioisotopes ^{60}Co or ^{137}Cs as a source[18], [24], [41], [42], [43], [44]. However, the radioisotope ^{137}Cs has greater advantages over ^{60}Co, as it has a longer half-life, greater stability in the radiation level supplied to the detector and, despite having a lower energy level, it reaches dimensions in materials that meet most measurement purposes[18]. Another advantage is the smaller shielding volume. A precision scan is more readily performed with low-energy sources because they require less shielding and, therefore, have less mass to be moved[21]. Another characteristic of the radioisotope ^{137}Cs is the fact that it is considered a source with a monoenergetic radiation beam, since the probability of emitting photons with an energy of 0.662 MeV is 85%[22].

In MCNP6, the source specifications are made in the mnemonic SDEF, which requires, among others, the following information: energy, position and type of particle emitted. The energy ("ERG") is always defined in MeV. The position ("POS") uses canonical coordinates x, y, z and must be complemented with the direction ("VEC") and sense ("DIR") of the particle flux[41]. The particle ("PAR") is defined as: "1" for neutrons, "2" for photons and "3" for electrons. Therefore, the source used in this paper has the following specifications: ERG= 0.662; DIR= 1; VEC= 1 0 0; PAR=2; POS= x y z. The latter is the only one that varies due to the scanning of the radiation beam along the pipeline.

2.4.2. Tally and NPS Specification

The calculation results are printed on the output file using tally, along with the relative error representing statistical accuracy. A normalization for the number of Monte Carlo histories is done on the results, so that the expected averages are independent of the number of source particles initiated in the MCNP calculation[28].

In this paper, the F1: p 8 tally will be used, which will record the relative intensity $\frac{I}{I_0}$ of the photons that will cross surface 8, normalized by the NPS (or number of stories). Surface 8 is in the input file the base of a cylinder defined as the face of the detector that faces the source (see example in Figure 9). The NPS defined for each pipeline considered a tally error of less than 1%.

2.5. Analysis of the presence of wax in the computational model

In this model, a percentage of 5% of the internal radius of the pipelines was established for the minimum thickness of wax to be detected. This percentage represents 4.3 mm for the smallest pipeline analyzed (8 inches) and 12.3 mm for the largest (24 inches). It is considered that the values are close to what has been reported in the literature, in which it was possible to measure wax thickness with an absolute precision of ± 5 mm, sufficient to ensure the reliable operation of the pipeline system[18]. Considering the importance of detecting the presence of wax before there is partial obstruction of the pipeline, a maximum thickness of 50% of its internal radius was also considered. For all pipelines, a length of 30 cm was adopted in the model.

For profiling the pipelines, a step of 4% of the external radius was established, such that there is the same number of points drawn in each profile, regardless of the diameter of the pipeline, as well as the same numerical identification of each position. In this way, 26 input files will be created for simulation, one for each beam position along the cross-section of the pipeline, starting from the outer edge and going halfway through, since the other half

is symmetrical because a concentric distribution of the wax layer is considered[5]. Due to the influence of seawater on the relative intensity records, a fixed distance of 0.5 cm was adopted between the source (or detector) and the edge of the pipeline in all beam positions.

With the records of the relative intensities calculated by MCNP6, several profiles were plotted, the first with the pipeline without wax (reference) and the others with thicknesses of 5, 10, 20, 30, 40, and 50% in relation to the inner radius. For each pipeline, a characteristic curve of the presence of wax was drawn using the relative intensities recorded at the positions of the gamma radiation beam that passes through the diameter of the pipeline. This decision was made sense during the analysis of the profiles it was noticed that the greatest differences in relative intensities between each profile with wax and the reference profile are in the positions that pass through the diameter.

2.6. Validation of the computational model

Considering that this research did not find experimental data in the literature on the detection of wax incrustation using a model consistent with that proposed in this paper, the validation was carried out using the experimental data where the gamma radiation transmission profiling technique was used with the radioisotope ^{137}Cs to identify the presence of $BaSO_4$ incrustation on the internal walls of a 450 mm diameter and 40 mm thick pipeline used in the oil and gas industry[45].

The experiment reported that the profiling of the pipeline was performed in 5 mm steps, without overlap between inspection points, and that a NaI(Tl) detector recorded the intensity of gamma radiation point by point, according to the thickness penetrated in the pipeline chord, thus obtaining a relative intensity $\frac{I}{I_0}$ profile as a function of the position of the gamma radiation beam[45]. The results showed that the pipeline was empty (filled with air) and contained a thickness of up to 21 mm of $BaSO_4$ incrustation. However, the accuracy of the counts at each step of the profile was not mentioned.

With this information, the input files were prepared with the application of the gamma radiation transmission profiling technique and the simulation was carried out in the computational model. The profile resulting from the MCNP6 calculations was then compared with the experimental profile.

3. RESULTS AND DISCUSSIONS

3.1. Results of the validation of the computational model

Figure 5 shows the experimental and simulated profile graphs in the computational model.

Figure 5 : Experimental and simulated profile plots

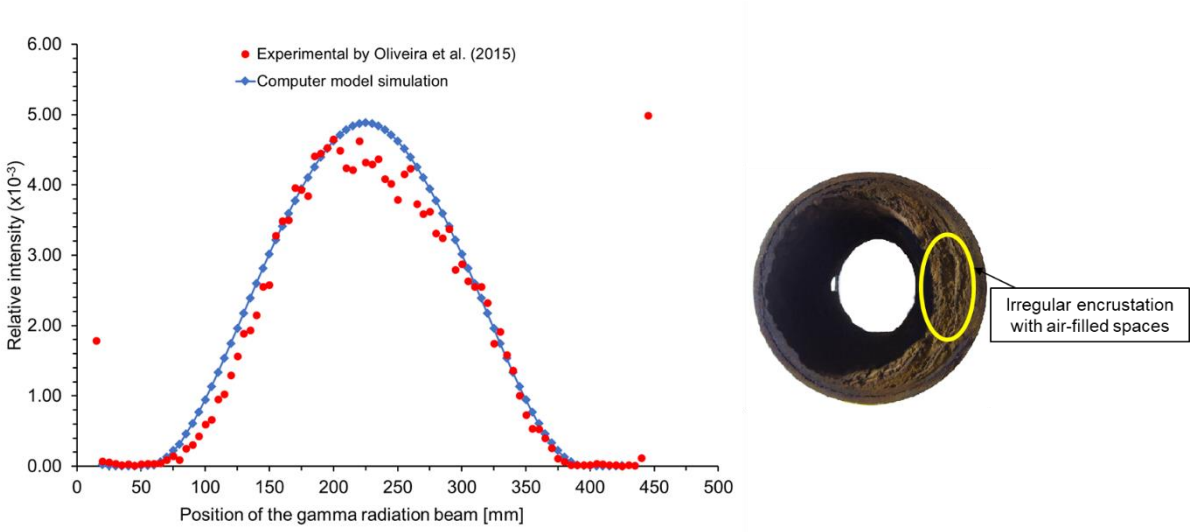

Source: Adapted from [45]

Figure 5 shows that there is similarity between simulated and experimental profiles, but there are differences at several points. These differences are due to the tendency of the incrustation to eccentric deposition, combined with the absence of material[24], indicating that the duct sample used in this experiment contains irregularities in the incrustation thickness, with some spaces filled with air, as shown in Figure 6[45]. Although it is not apparent in the graph, the greatest differences are in the beam position ranges from 15 to

120 mm and 350 to 440 mm, which make up the region where the gamma radiation beam travels through the interior of the duct wall and the thickness of the $BaSO_4$ incrustation, both on the upper and lower sides. Therefore, disregarding the experimental data from these ranges where the greatest differences with the simulated data occur, the rest of the experimental data were fitted to a Gaussian curve (Equation 6).

$$y = y_o + \frac{A}{w \times \sqrt{\frac{\pi}{4 \times \ln 2}}} \times e^{\left(-4 \times \ln 2 \times \frac{(x - x_c)^2}{w^2}\right)}, \quad R^2 = 0.97786 \tag{6}$$

Where: $y_0 = -7.93866 \times 10^{-4}$; $x_c = 225.69387$; $A = 1.09764$; $w = 193.05101$

Figure 6 shows the experimental profile plot, the Gaussian fitting curve and the profile simulated in the computational model.

Figure 6 : Fitting curve of the experimental profile versus the computational model profile

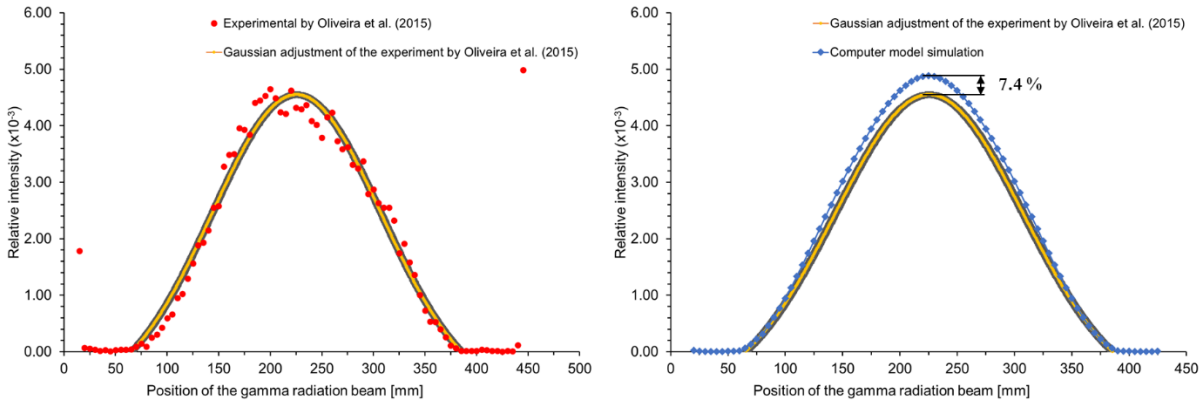

It can be observed that the curves have the same behavior as Gaussian curves whose peaks are coincidence. The peak of the curve obtained in MCNP6 has a greater amplitude due to the simplifications inherent to the computational model. The greatest difference between the curves occurs in the central region that corresponds to the diameter of the duct. This difference provides a maximum relative error of 7.4%.

3.2. Analysis of the presence of wax in oil pipelines

An analysis of the presence of wax was carried out on the 8-inch pipeline in Table 6. This pipeline was profiled at a 4.4 mm step, which represents 4% of the external radius, as established. With the relative intensity values and the positions of the gamma radiation beam, the transmission profiles were drawn, as shown in Figure 7.

Figure 7 : Profiling the 8-inch pipeline with pre-set layers of wax

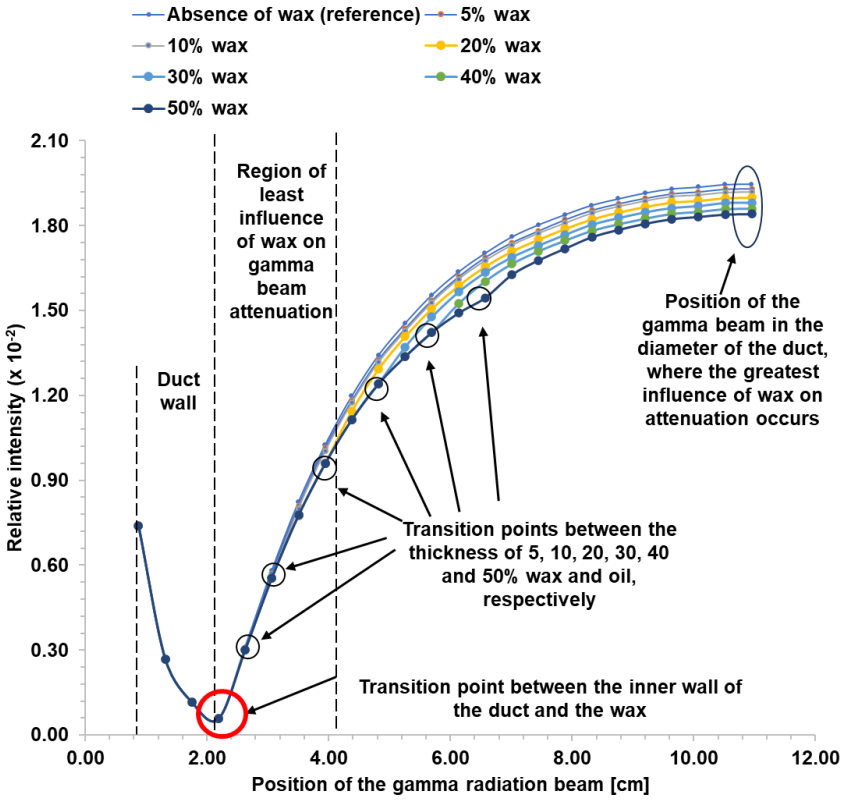

Figure 7 shows that the region of the pipeline wall causes the greatest attenuation of the gamma radiation beam, given that the density of the pipeline (composed of approximately 95% iron) is 8.5 times greater than the density of wax. The relative intensity begins to increase after the gamma radiation beam passes the transition point between the inner wall of the duct and the wax (highlighted in the red circle of the graph in Figure 7), where differences between the profiles begin to appear. These differences are due to the influence of the wax on the inner wall of the pipeline. During the 5, 10, 20, 30, 40 and 50% wax profiles, you can

see the transition points between the thickness of the wax and the oil, characterized by a small jump[38]. On the other hand, at positions close to the diameter of the pipeline, the difference between each profile and the reference profile is greater. In the position that passes through the diameter, therefore, is where the greatest influence of wax occurs, with a greater chance of wax being detected. Based on this analysis, the characteristic curves for the presence of wax for all the pipelines were plotted with the relative intensity records at the position passing through the diameter.

3.3. Characteristic curves for the presence of wax

The characteristic curves were drawn according to the analysis in the previous section. In addition, as stated in section 2.4.2, the NPS was estimated in such a way that it is possible to detect the minimum wax thickness, i.e. 5% of the internal radius of the pipeline within a confidence interval equal to or greater than one standard deviation.

Figure 8 shows the relative intensities calculated for the 8-inch pipeline and the corresponding characteristic curve.

Figure 8 : Characteristic curve of the presence of wax in the 8-inch pipeline with application of 10 millions stories

Percentage of inner radius [%]	Wax thickness [cm]	Relative Intensity ($x10^{-2}$)	Tally error	Standard deviation
0	0.00	1.95	0.0022	4.28E-03
5	0.43	1.93	0.0023	4.44E-03
10	0.87	1.92	0.0023	4.41E-03
20	1.73	1.90	0.0023	4.37E-03
30	2.60	1.88	0.0023	4.33E-03
40	3.46	1.86	0.0023	4.28E-03
50	4.33	1.84	0.0023	4.23E-03

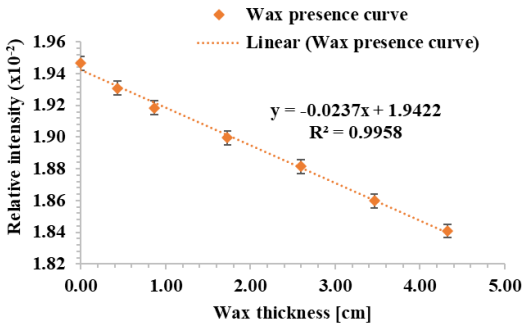

Figure 9 shows the input file used to calculate the relative intensity of 5% wax in the 8-inch pipeline (see Table in Figure 8).

Figure 9 : Input file for calculating the relative intensity of 5% wax in the 8-inch pipeline with application of 10 millions stories

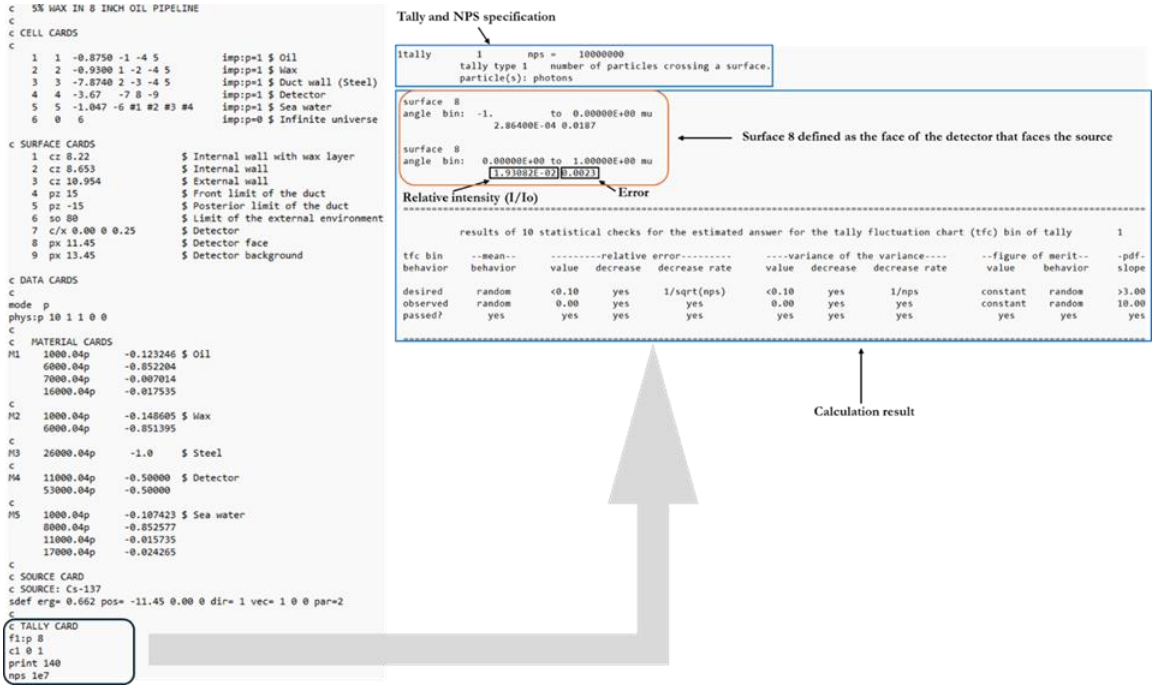

This was also done for the other pipelines in Table 6 (Figure 10).

Figure 10 : Characteristic curves for the presence of wax in 12-, 16-, 20- and 24-inch pipelines

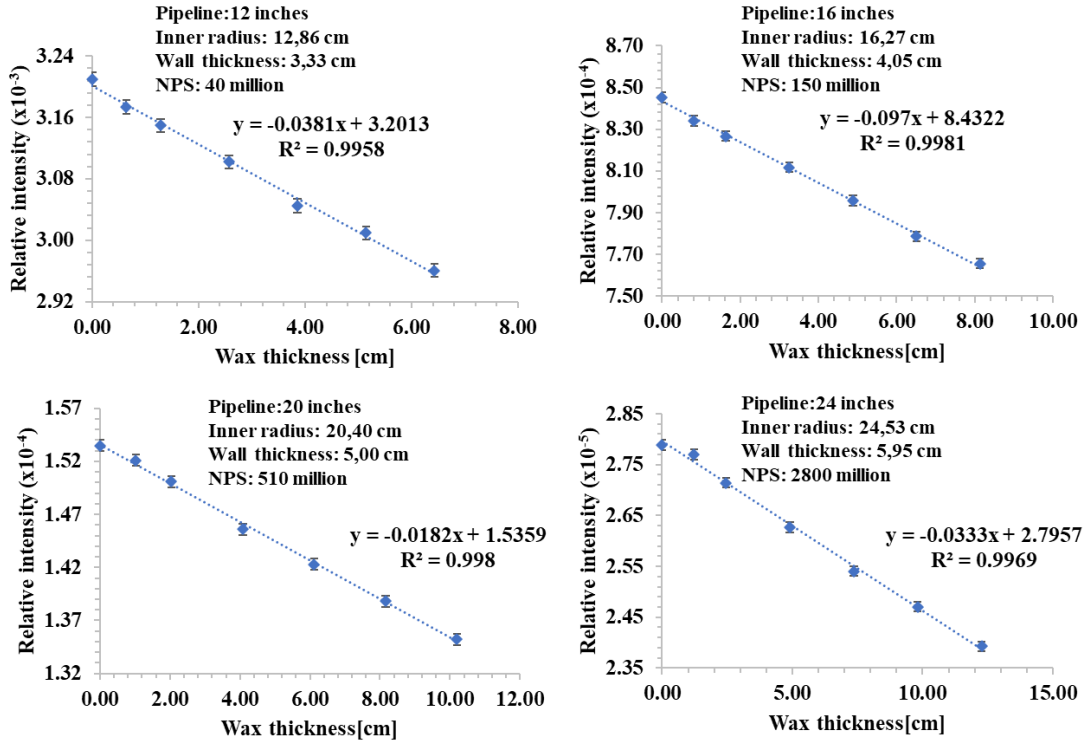

4. CONCLUSIONS

A computational model of a deepwater subsea oil pipeline was developed in the MCNP6 code, where the gamma radiation transmission profiling technique was applied. The model was shown to be consistent with experimental data in the literature, with a maximum relative error of 7.4% in the position passing through the diameter of the pipeline. Using the model, profiling was carried out on a pipeline used in the oil industry to detect the presence of wax on its internal walls. Analyses carried out in different regions of the pipeline showed that wax was more likely to be detected in the position of the beam that passes through the diameter of the pipeline.

With the simulated relative intensity readings at the position of the diameter, characteristic curves for the presence of wax were drawn for each pipeline and the numerical accuracy of the results was analyzed, where it was necessary to estimate the number of histories to achieve an accuracy such that the readings for the absence and presence of wax were distinct.

The results of this study showed that the model developed can detect up to 5% wax (in relation to the internal radius of the pipeline) in all the pipelines analyzed, within a confidence interval equal to or greater than one standard deviation.

ACKNOWLEDGMENT

The authors would like to thank the Northeast Regional Nuclear Science Center (CRCN-NE/CNEN).

CONFLICT OF INTEREST

All authors declare that they have no conflicts of interest.

REFERENCES

[1] MATOS, S. F.; ALTOÉ, L. Analysis of deepwater oil flow assurance in relation to wax deposition. Latin American Journal of Energy Research, vol. 6, no 2, p. 12–31, 2020, doi: 10.21712/lajer.2019.v6.n2.p12-31.

[2] PORTO, T. R. N.; LIMA, A. G. B. De. Transient flow of waxy oil in a circular section pipeline: modeling and simulation, Holos, vol. 1, p. 155–173, 2017, doi: 10.15628/holos.2017.5220.

[3] AL-YAARI, M. wax deposition: mitigation and removal techniques. Society of Petroleum Engineers, p. 14–16, 2011.

[4] THEYAB, M. A. Wax deposition process: mechanisms, affecting factors and mitigation methods. Open Access Journal of Science, vol. 2, no 2, mar. 2018, doi: 10.15406/oajs.2018.02.00054.

[5] MATZAIN, A.; APTE, M. S.; ZHANG, H. Q.; VOLK, M.; BRILL, J. P.; CREEK, J. L. Investigation of paraffin deposition during multiphase flow in pipelines and wellbores - Part 1: Experiments. Journal of Energy Resources Technology, Transactions of the ASME, vol. 124, no 3, p. 180–186, set. 2002, doi: 10.1115/1.1484392.

[6] BORDALO, S. N.; OLIVEIRA, R. Biphasic oil-water flow with wax precipitation in subsea oil production pipelines, 4° Congresso Brasileiro de Petróleo e Gás - PDPETRO, Campinas, São Paulo: Associação Brasileira de Pesquisa e Desenvolvimento em Petróleo e Gás - ABPG , out. 2007, p. 12.

[7] CHEN, X. T.; BUTLER, M.; VOLK, M. Techniques for measuring wax thickness during single and multiphase flow, SPE Annual Technical Conference and Exhibition, San Antonio, Texas: Society of Petroleum Engineers, out. 1997, p. 1–8.

[8] VIANA, C. PIG Passage - Critical Operation: Concepts, Operations and Recommendations, LinkedIn. Accessed: May 30, 2023. [Online]. Available at: https://www.linkedin.com/pulse/passagem-de-pig-operação-crítica-conceitos-operações-viana/?originalSubdomain=pt

[9] MORAIS, J. M. Deepwater Oil: A Technological History of PETROBRAS in Offshore Exploration and Production. Brasília: PETROBRAS, 2013.

[10] MAJID, S. A.; MELAIBARI, A; MALKI, B. Hydrocarbon scale deposits measurements by neutron moderation and capture gamma methods, Nuclear Instruments and Methods in Physics Research B, vol. 119, p. 433–437, 1996.

[11] HOFFMANN, R.; AMUNDSEN, L.; SCHÜLLER, R. Online monitoring of wax deposition in sub-sea pipelines, Meas Sci Technol, vol. 22, no 7, 2011, doi: 10.1088/0957-0233/22/7/075701.

[12] CHEN et al., H. Ultrasonic detection and analysis of wax appearance temperature of kingfisher live oil, Energy and Fuels, vol. 28, no 4, p. 2422–2428, abr. 2014, doi: 10.1021/ef500036u.

[13] MEI, I. L. S.; ISMAIL, I.; SHAFQUET, A.; ABDULLAH, B. Real-time monitoring and measurement of wax deposition in pipelines via non-invasive electrical capacitance tomography, Meas Sci Technol, vol. 27, no 2, dez. 2015, doi: 10.1088/0957-0233/27/2/025403.

[14] SOARES, L. L. O. Determination of the onset of paraffin deposition in oil production and transportation pipelines using a Multipoint Temperature Sensor. Federal University of Bahia, Polytechnic School, Salvador, 2017.

[15] OLIVEIRA, A. A. Historical success stories in the use of MAD-pig to locate obstructions in pipelines, Technical Bulletin of Oil Production, vol. 1, no 1, Rio de Janeiro, p. 95–126, 2006.

[16] KOPTEVA, A.; KOPTEV, V.; MALAREV, V.; USHKOVA, T. Development of a system for automated control of oil transportation in the Arctic region to prevent the formation of wax deposits in pipelines, Proceedings of EECE 2019: Energy, Environmental and Construction Engineering, St. Petersburg, Russia: EDP Sciences, nov. 2019. doi: 10.1051/e3sconf/201914007004.

[17] LOPES, R. T.; VALENTE, C. M.; DE JESUS, E. F. O.; CAMERINI, C. S. Detection of paraffin deposition inside a draining tubulation by the Compton Scattering Technique, Applied Radiation and Isotopes, vol. 48, no 10–12, p. 1443–1450, 1997, doi: 10.1016/S0969-8043(97)00255-8.

[18] KOPTEVA, A.; STARSHAYA, V. Radioisotope measuring system for oil stream asphaltene-resin-paraffin deposits ARPD parameters. SPE Russian Petroleum Technology Conference and Exhibition, Moscow, Russia: Society of Petroleum Engineers, out. 2016, p. 1–7.

[19] ABDUL-MAJID, S. Determination of wax deposition and corrosion in pipelines by neutron back diffusion collimation and neutron capture gamma rays, Applied Radiation and Isotopes, vol. 74, p. 102–108, abr. 2013, doi: 10.1016/j.apradiso.2013.01.012.

[20] TAUHATA, L.; SALATI, I.; PRINZIO, R. D.; PRINZIO, A. R. D. Radioprotection and Dosimetry: Fundamentals, 10o ed. Rio de Janeiro: Comissão Nacional de Energia Nuclear, 2014.

[21] JOHANSEN, G. A.; JACKSON, P. Radioisotope Gauges for Industrial Process Measurements. Southern Gate, Chichester: John Wiley & Sons, 2004.

[22] KNOLL, G. F. Radiation Detection and Measurement, 4o ed. Ann Arbor, Michigan: John Wiley & Sons, 2010.

[23] LEITE, N. M.; LIRA, C. A. B. O.; RODRIGUEZ, A. G. Computational analysis for wax detection in deepwater pipelines using nuclear techniques. Brazilian Journal of Radiation Sciences, vol. 11, no 1A (Suppl.), p. 1–20, jul. 2023, doi: 10.15392/2319-0612.2023.2193.

[24] BESERRA, M. T. F. Assessment of scale thickness in oil extraction pipelines. Institute of Radiation Protection and Dosimetry, Rio de Janeiro, 2012.

[25] SOARES, M. Fouling Detection System in Oil Pipelines Using Gamma Transmission Technique. Federal University of Rio de Janeiro, Rio de Janeiro, 2014.

[26] YORIYAZ, H. Monte Carlo Method: principles and applications in Medical Physics. Brazilian Journal of Medical Physics, vol. 3, no 1, p. 141–149, 2009.

[27] GOORLEY, J. T.; JAMES, M. R.; BOOTH, T. E.; BROWN, F. B.; BULL, J. S.; COX, L. J.; DURKEE, J. W. J.; ELSON, J. S.; FENSIN, MICHAEL LORNE FORSTER, ROBERT A. III HENDRICKS, J. S.; HUGHES, H. G. I.; JOHNS, R. C.; KI, A. J. Initial MCNP6 release overview -MCNP6 version 1.0. Los Alamos: Los Alamos National Laboratory, 2013.

[28] LOS ALAMOS NATIONAL LABORATORY. Monte Carlo N–Particle Transport Code System Including MCNP6.1, MCNP5-1.60, MCNPX-2.7.0 and Data Libraries. Los Alamos, New Mexico: Radiation Safety Information Computational Center, 2013.

[29] JOHANSEN, G. A.; JACKSON, P. Salinity independent measurement of gas volume fraction in oil/gas/water pipe flows, Applied Radiation and Isotopes, vol. 53, p. 595–601, 2000, [Online]. Disponível em: www.elsevier.com/locate/apradiso

[30] SALGADO, C. M. Identification of Flow Regimes and Prediction of Volume Fractions in Multiphase Systems Using Nuclear Technique and Artificial Neural Network. Federal University of Rio de Janeiro, Rio de Janeiro, 2010.

[31] YEH, M. K.; KYRIAKIDES, V. Collapse of Deepwater Pipelines. 18th Offshore Technology Conference, Houston, Texas: American Society of Mechanical Engineers, maio 1986.

[32] GOUVEIA, J. C. C. Critical engineering analysis for rigid pipes submitted to large deformations. Rio de Janeiro: Fluminense Federal University, 2010.

[33] TUBOS ABC, API 5L tubes grades X42 to X80. ABC Tubes. Acessado: 20 de maio de 2022. [Online]. Disponível em: https://www.tubosabc.com.br/tubos/tubos-api-5l/?doing_wp_cron=1684622473.7044830322265625000000

[34] TYCOON PIPING SOLUTION. API 5L X65 PSL2 Pipe. Acessado: 13 de julho de 2023. [Online]. Disponível em: https://www.oilandgaspipingmaterials.com/iso-3183-l450-api5l-x65-psl1-psl2-pipe-suppliers.html

[35] MCCONN, R.; GESH, C.; PAGH, R.; RUCKER; WILLIAMS, R. Compendium of material composition data for radiation transport modeling. Washington: Pacific Northwest National Laboratory, 2011.

[36] NATIONAL AGENCY OF PETROLEUM, NATURAL GAS AND BIOFUELS, Oil and Natural Gas Production Bulletin No. 152. Acessado: 25 de junho de 2023. [Online]. Disponível em: https://www.gov.br/anp/pt-br/centrais-de-conteudo/publicacoes/boletins-anp/boletins/arquivos-bmppgn/2023/boletim-abril.pdf

[37] NATIONAL AGENCY OF PETROLEUM, NATURAL GAS AND BIOFUELS, Oil and Natural Gas Production Bulletin No. 121. Acessado: 1o de fevereiro de 2023. [Online]. Disponível em: https://www.gov.br/anp/pt-br/centrais-de-conteudo/publicacoes/boletins-anp/boletins/arquivos-bmppgn/2020/boletim-12-2020.pdf

[38] MALAREV, V. I.; KOPTEVA, A. V. Using radioisotope method for measuring ice layer thickness in pulp lines. IOP Conf Ser Earth Environ Sci, vol. 87, no 3, 2017, doi: 10.1088/1755-1315/87/3/032022.

[39] DOBBS, J. B. A unique method of wax control in production operations. SPE Rocky Mountain Regional Meeting, Gillette, Wyoming: Society of Petroleum Engineers Inc, maio 1999, p. 1–6.

[40] FERREIRA, C. A. M. Detection of annular flooding in flexible ducts using the gamma radiation transmission technique. Federal University of Rio de Janeiro, Rio de Janeiro, 2021.

[41] GUEDES, K. A. N. Simulation using the MCNPX code for gamma tomography and validation with experimental data. Federal University of Pernambuco, Recife, 2016.

[42] MCCAW, D. D.; HULBERT, V. G.; SMITH, A. E. Gamma scanning of large sieve tray towers". NUCLEX 75: International Nuclear Industries Fair and Technical Meeetings, Basel, Switzerland: Atomic Energy of Canada Limited, out. 1975, p. 1–13.

[43] CARNEIRO JUNIOR, C. Development of a Gamma Transmission-Based Inspection System for Application in Flexible Pipes and Industrial Columns. Federal University of Rio de Janeiro, Rio de Janeiro, 2005.

[44] TEIXEIRA, T. P. Prediction of scale thickness in pipelines used in oil transportation using gamma radiation and artificial neural network. Institute of Nuclear Engineering, Rio de Janeiro, 2018.

[45] OLIVEIRA, D. F.; NASCIMENTO, J. R.; MARINHO, C. A.; LOPES, R. T. Gamma transmission system for detection of scale in oil exploration pipelines. Nuclear Instruments and Methods in Physics Research A, vol. 784, p. 616–620, jun. 2015, doi: 10.1016/j.nima.2014.11.030.

LICENSE